A Significant Role of MoO3 on the Optical, Thermal, and Radiation Shielding Characteristics of B2O3-P2O5 -Li2O Glasses

kh. S. Shaaban (✉ khamies1078@yahoo.com)

faculty of science al azhar university at assiut   https://orcid.org/0000-0002-5969-3089

A Significant Role of MoO$_3$ on the Optical, Thermal, and Radiation Shielding Characteristics of B$_2$O$_3$-P$_2$O$_5$ -Li$_2$O Glasses

Kh. S. Shaaban[1],

[1]Chemistry Department, Faculty of Science, Al-Azhar University, P.O. 71452, Assiut, Egypt

ABSTRACT

Glasses based on borophosphate with the formula $42.5P_2O_5 – 42.5B_2O_3 – (15\text{-}x) Li_2O – xMoO_3$ mol% where $x = (0 \leq x \geq 15)$ were manufactured using the melt-quenching methodology. The status of prepared samples was identified by (XRD). The temperature of the glass transition T_g, the temperature of onset glass crystallisation T_c and the temperature of the crystallisation T_p were evaluated using a differential thermal analyser (DTA). The energy gap (E_{opt}), Urbach (E_u), and parameters of dispersion were calculated through the data of optical spectra. Physical properties were determined and calculated, such as molar refractivity, metallization, electron polarizability, electronegativity, loss of reflection and dispersion parameters. Raising MoO$_3$ at the expense of Li$_2$O was used to assess the level of protection. For radiation protection applications, the glasses under investigation had superior characteristics.

Keywords: MoO$_3$, XRD Spectroscopic, DTA, Attenuation.

*Corresponding Author: Email: <u>khamies1078@yahoo.com</u>

1. Introduction

B_2O_3-P_2O_5 glasses with superior efficiency can be used in a variety of different settings. Solid-state batteries, and nonlinear optics borophosphate glasses are appropriate. Due to its obvious advantages, lithium borophosphate is classical glass that has become recognized in storage batteries. These glasses are used as storage batteries in optical and electronic instruments. The addition of modifiers such as Li_2O influences of these characteristics. Li_2O will be combined instead of B-change BO_4 to BO_3 [1-8]. The characteristics of the combined glass (B_2O_3+P_2O_5) networks vary from those of the single glass B_2O_3 and P_2O_5 networks.

Transition metal oxides (TMOs) are a fascinating group of semiconductor materials because of their technological advantages for use in microelectronics and display systems. MoO_3 among (TMOs), due to its excellent use in optical materials and electrochemical devices has received increasing attention in recent years. There is a goal that support in manufacturing these glasses regarding the MoO_3 used in these implementations. Different MoO_3 preparation glasses were developed and investigated in response to this broad range of applications [9-16].

Due to the existence of MoO_4 and MoO_6 in the glass network, MoO_3 appears as the former non-conventional network. The existence of MoO_3 in glass systems does have a modifier impact on UV spectra [9-16]. There are increasingly diverse technologies for molybdenum borophosphate-based glasses, such as laser host fibers and superconducting switches.

Both scientifically and technologically, the significant advances of alkaline borophosphate glasses are considerable. The existence of PO_4 & BO_4 structural units, this consequence approaches from the structural issues connected with covalent links. In several fields, B_2O_3-P_2O_5 - Li_2O - MoO_3 glasses possess high applications because of their radiation shielding and good FT-IR transmission [17-33]. The object of this study is to assist you in the

preparation of B_2O_3-P_2O_5 - Li_2O - MoO_3 glasses and investigating their optical and neutron shielding using Phy-X/PSD [34] properties.

2. Methodology

Table 1 shows how we formed the glasses in our published articles using the melt-quenching methodology. By melting together of B_2O_3 in its H_3BO_4 (Merck), Li_2O in it Li_2CO_3 (Aldrich), P_2O_5 in it $(NH_4)_2HPO_4$ (Merck) and MoO_3 (Merck) in an o pen ceramic crucible. With the evaporation of CO_2, NH_3 and H_2O, Li_2CO_3, $(NH_4)_2HPO_4$ and H_3BO_4 and are converted into Li_2O, P_2O_5 and B_2O_3. The furnace temperature was changed at a melting temperature of 1050 °C. At 350 °C the prepared samples are annealed.

The Philips X-ray diffractometer (model PW / 1710) checked the condition of these glasses and glass-ceramics. The spectrophotometer was used to measure the optical spectra of the investigated glass system (type JASCO V- 670). The thermal investigation was carried out with a DTA-50 (Shimadzu-Japan). Phy-X / PSD can calculate a variety of shielding considerations [34]. Electron density (N_{eff}) was predictable as: $N_{eff} = N \frac{Z_{eff}}{\sum_i F_i A_i}$,. Effective cross-section of removal (Σ_R) projected as: $\left(\frac{\Sigma_R}{\rho}\right) = \sum_i w_i \left(\frac{\Sigma_R}{\rho}\right)_i$ and $R = \sum_i \rho_i \left(\frac{R}{\rho}\right)_i$,. G–P fitting parameters has been predictable as $P = \frac{P1(\log Z2 - \log Zeq) + Z2(\log Zeq - \log Z1)}{\log Z2 - \log Z1}$. EABF and EBF were predictable using G–P fitting $B(E, X) = 1 + \frac{b-1}{K-1}(K^x - 1)$ for $K \neq 1$, $B(E, X) = 1 + (b-1)x$ $K = 1$ where $K(E, X) = cx^a + d \frac{\tanh(\frac{x}{Xk} - 2) - \tanh(-2)}{1 - \tanh(-2)}$

3. Results and Discussion

3.1. XRD

Figure 1 depicts the glass system's X-ray features. In the glass samples, XRD revealed no discrete lines or sharp peaks, indicating a high degree of glass status.

3.2 Optical spectra

3

The absorption (A), transmittance (T), and reflectance (R) of glass samples are shown in Figures 2 and 3. Spectral UV according to reports, increasing. As a result, MoO_3 is to blame for the slight increase in BO [35-44]. Figure 4 shows the absorption coefficient of the glasses.

3.2.1 band gap E_{opt}

Glass spectrum in the UV and VIS areas were used for the estimated of the band gap energy E_{opt} is estimated by $(\alpha.h\nu)^{1/2} = B(h\nu - E_{opt}.)$ where B is an energy independent constant and $h\nu$ is photon energy. By intrigue the $(\alpha.h\nu)^{1/2}$ versus $h\nu$ as Fig.5. Plot of $(\alpha.h\nu)^{1/2}$ against photon energy $(h\nu)$ to evaluate the indirect E_{opt} from the intercept. E_{opt} increases with increasing MoO_3, as revealed in Table 2, due to oxygen bridges (BO) form and bind excited electrons more tightly than non-bridging oxygen electrons (NBO). Urbach energy has been calculated $\propto_0 exp\left(\frac{h\nu}{E_u}\right)$, Fig. 6 and table 2 show that their E_{opt} values have an inverse relationship. The values of E_{opt} and E_u

 was shown in Fig.7.

The refractive index was calculated using: $n = \frac{(1-R)^2 + k^2}{(1+R)^2 + k^2}$ where $k = \alpha\lambda/4\pi$. The refractive index presented in Fig.8 for fabricated glasses. It has already been stated that density increase, the refractive index of these samples increased. As a result, it can be directly compared to reflectance and density, and opposite to molar volume.

3.2.2 Dispersion parameters

As approximated, molar polarization and polarizability of glasses were computed :

$$R_m = \langle n^2 - 1 | n^2 + 2 \rangle Vm, \quad \propto_m = (3|4\pi N)R_m, \quad \text{and} \quad \propto_0^{2-} = \frac{[\frac{Vm}{2.52}\left(\frac{n^2-1}{n^2+2}\right) - \Sigma\propto_{cat}]}{N_o^{2-}} \qquad \textbf{[45-49]}.$$

Polarization was linked with the optical basicity; $\Lambda = 1.67\left(1 - \frac{1}{\propto_0^{2-}}\right)$. Figs. 9,10& 11 exemplifies the polarizabilities, Molar Polarizability $\propto_m$ and optical basicity separately of the

samples. The refractive index is trending in the same direction with MoO_3 content has been reported to enhance.

The molar refractivity as $E_{opt.}$ $R_m = Vm\left(1 - \sqrt{Eg/20}\right)$ and molar polarizability $(\propto_m)$ $\propto_m = \left(\frac{3}{4\pi N}\right) R_m$. Reflection loss $R_L = \left(\frac{R_m}{Vm}\right)$. Because the molar volume decreases with Mo^+, these values of (R_m) $(\propto_m)$ and (R_L) decline. The criterion for metallization is predicted as $M = 1 - \frac{R_m}{Vm}$, the metallization value increase with Mo^+. The electronegativity (χ) is predicted as $\chi = 0.2688E_{opt.}$ where $E_{opt.}$ bandgap. Thus, with Mo^+ increasing, the electronegativity (χ) values increase. The electron polarizability is predicted as, $\propto^\circ = -0.9\,\chi + 3.5$ and optical basicity $\wedge = -0.5\chi + 1.7$. $\propto^\circ$ and $\wedge$ have the opposite value of (χ) so, $\propto^\circ$ and $\wedge$ decrease with Mo^+. These items are obtainable in Table 2.

The dispersion was calculated by Wemple and Didomenico E_o and E_d [50-53]. The hypnosis designates explained by $n^2 - 1 = \frac{E_0\,E_d}{E_0^2 - E^2}$ [64-70]. The plotting of, $(n^2-1)^{-1}$ with $(hʋ)^2$ E_o and E_d predictable from the slope and intercept as shown in Figs. 12 & 13. It mentioned that with increasing MoO_3, E_o and E_d were slightly enhanced. The optical energy E_{opt} that represent $Eopt = \frac{E_d}{2}$. Refractive Static index at infinite wavelength (n_o) was estimated by $n_0 = \sqrt{1 + \frac{E_d}{E_0}}$ and the static dielectric $\varepsilon_\infty = n_0^2$. The oscillator's wavelength (λo) and strength (S_o) were calculated using the following formula $n^2 - 1 = \frac{S_0\,\lambda_0^2}{1 - (\frac{\lambda_0}{\lambda})2}$. These items are obtainable in Table 3.

3.3 DTA

The thermal analysis (DTA) of glass samples demonstrated in Fig. 14. The temperature of the glass transition, Tg, is 493-532 ±3 °C. The temperature of the glass crystallisation T_c starts at 537-580 ±3 °C. The temperature of the glass crystallisation T_c ends at 606-645 ±3 °C. According to DTA observations, Tg increases from 493 into 532 °C, Tc increases from 537

into 580 °C and Tp increases from 606 into 645 °C with the increase of MoO_3 content. The transformation of Li-O to Mo-O linkages is significantly associated with this behaviour. Hence, Li−Li (137.3±6.3 KJ/mol) dissociation energy is weaker than Mo−Mo (449.4±1 KJ/mol) dissociation energy and adding MoO_3 variations the basic B units from BO_3 to BO_4. Thermal stability estimated by $\Delta T = (Tc - Tg)$, weighted thermal stability $Hg = \Delta T/Tg$ and $S = (Tp - Tc) \Delta T/Tg$. It observed that all thermal stability of samples improved as MoO_3. The T_g, T_c, T_p and thermal stability values are obtainable in Table 4.

3.4 Photon Shielding Features

The level of protection was assessed in this article by increasing MoO_3 at the expense of Li_2O with the composition $42.5B_2O_3 - 42.5P_2O_5 - (15 - x)Li_2O - xMoO_3$, $(0 \leq x \geq 15)$. The mean free path (MFP) is depicted in Fig.15. It was stated that as photon energy increases, the values of (MFP) increase. This insight revealed that as the photon's energy increases, it becomes capable of transmitting samples on purpose. Because the lower value of the (MFP) sample has a higher MoO3 content, good radiation attenuation glasses are available. [54-71].

Figure 16 demonstrations the (N_{eff}) of fabricated glasses. It is demonstrated that (N_{eff}) decreases and then rises as energy increases. This significant decrease can be attributed to the interaction of Compton scattering. The effect of forming pairs at higher energy levels as MoO_3 is linked to the increasing in (N_{eff}).

The ASC of fabricated glasses are presented in Fig. 17. The ASC and ESC values are expected to decrease as energy rates increase. This decrease occurs due to the Compton scattering interaction. The C_{eff} of fabricated glasses depicted in Figure 18. With the increase in photon energy, it is predicted that C_{eff} will decrease. The impact of pair-creation was reflected in the increase in C_{eff}.

6

The EBF & EABF of fabricated glasses were characterized by Figs. 19&20. EBF and EABF values are determined by the lower energy and concentration of the glass samples. At lower energy levels, EBF and EABF values are low, but they rise as energy levels rise. After that, gradually decrease as energy level rises. So, we can divide the energy scale into three parts low, medium, and high. The first part (low energy): the typical phase is the photoelectric effect, and the relationship is reversed with light, and the glasses will absorb the energy photons. The photons are therefore not allowed to build-up. In the second part (medium energy): the common process is the Compton scattering, the values of EBF and, EABF is increased in all samples independent from the MFP. Through this part, the photons stay in the samples for a long time, as these processes lead to high accumulation value due to multiple scattering processes. Third parts (high energy): the common process is the pair production. In this process, EBF and, EABF is decreased with energy. Therefore, these data helped in the determination of maximum radiation intensity occur. In this research, highest radiation occurs on the surface of the sample. In Fig. 21, fast cross section neutron removal (FNRCS) is shown. It was stated that MoO3 improved FNRCS.

4. Conclusions

In the existing research, molybdenum lithium borophosphate glasses $42.5P_2O_5 - 42.5B_2O_3 - (15-x) Li_2O - xMoO_3$ where $x = (0 \leq x \geq 15)$ were fabricated with conventional melt-quenching procedures. The optical, thermal, and shielding factors were observed. The findings showed the following objects:

1- Because of the increase in MoO_3, the metallization of these glasses was improved.

2- The 2.23 for G 1, 2.32 for G 2, 2.38 for G 3, 2.41 for G 4, and 2.49 for G 5 were identified as the indirect optical bands that were collected.

3- Urbach energies of these samples were reduces as the content of MoO_3 increase.

4- As the density of the investigated glasses rises, the refractive index rises as well.

5- These glasses were investigated for molar polarization, polarizability, and optical basicity.

6- T_g, T_c, T_p and thermal stability values are enhanced with MoO_3.

7- The fabricated samples' gamma shielding features were predictable. The impact of adding MoO_3 to the glasses on their shielding ability was mentioned.

8- Lower value of the (MFP) sample has more MoO_3 are good radiation attenuation glasses are available.

9- As the concentration of MoO_3 increased, these glasses have a high cross section neutron removal rate.

The findings discovered that as MoO_3 increase the glass system can result in significant improvements in attenuation and optical characteristics. Furthermore, it is possible to use this glass in optoelectronic, optical devices, and a radiation shield for use in x-ray centers.

References

[1] Narwal, P., Dahiya, M. S., Kundu, P., Yadav, A., Hooda, A., & Khasa, S. Compositional dependence of properties in calcium substituted sodium borophosphate glasses containing VO^{2+} ions. Bulletin of Materials Science, 42(3),105-113, (2019), DOI:10.1007/s12034-019-1812-6

[2] Khafagy, A. H., El-Adawy, A. A., Higazy, A. A., El-Rabaie, S., & Eid, A. S. Studies of some mechanical and optical properties of (70−x) TeO_2-15B_2O_3-15P_2O_5-xLi_2O glasses. Journal of Non-Crystalline Solids, 354(27), 3152–3158. (2008). DOI: 10.1016/j.jnoncrysol.2008.01.013

[3] Kim, D., Hwang, C., Gwoo, D. *et al.* Effect of titanium on structure of sodium borophosphate glasses. Electron. Mater. Lett. **7,** 343–347 (2011). https://doi.org/10.1007/s13391-011-0710-x

[4] Reddy, A. A., Babu, S. S., Pradeesh, K., Otton, C. J., & Vijaya Prakash, G. Optical properties of highly Er3+-doped sodium–aluminium–phosphate glasses for broadband 1.5μm emission. Journal of Alloys and Compounds, 509(9), 4047–4052. (2011). DOI: 10.1016/j.jallcom.2011.01.016

[5] Shaaban, K.S., Yousef, E.S., Mahmoud, S.A. et al. Mechanical, Structural, and Crystallization Properties in Titanate Doped Phosphate Glasses. J Inorg Organomet Polym (2020). https://doi.org/10.1007/s10904-020-01574-x

[6] Shaaban, K.S., Wahab, E.A.A., Shaaban, E.R., et al. Electronic polarizability, optical basicity, and mechanical properties of aluminum lead phosphate glasses. Opt Quant Electron **52,** 125 (2020). https://doi.org/10.1007/s11082-020-2191-3

[7] Fayad, A.M., Shaaban, K.S., Abd-Allah, W.M. *et al.* Structural and Optical Study of CoO Doping in Borophosphate Host Glass and Effect of Gamma Irradiation. J Inorg Organomet Polym (2020). https://doi.org/10.1007/s10904-020-01641-3

[8] El-Maaref, A. A., Shimaa Badr, Shaaban, K. S., Wahab, E. A. A., & El Okr, M. M. Optical Properties and Radiative Rates of Nd^{3+} Doped Zinc-Sodium Phosphate Glasses. Journal of Rare Earths. 37, 253-259 (2019). DOI: 10.1016/j.jre.2018.06.006

[9] Raza, S. H., Afzal, N., Rafique, M., Imran, M., & Ahmad, R. Structural and morphological properties of annealed MoO_3 films on different substrates. Surface Review and Letters. (2019). DOI:10.1142/s0218625x19501506

[10] Santagneli, S. H., de Araujo, C. C., Strojek, W., Eckert, H., Poirier, G., Ribeiro, S. J. L., & Messaddeq, Y. Structural Studies of $NaPO_3-MoO_3$ Glasses by Solid-State Nuclear Magnetic Resonance and Raman Spectroscopy. The Journal of Physical Chemistry B, 111(34), 10109–10117. (2007). DOI:10.1021/jp072883n

[11] Sivakumar, R., Manisankar, P., Jayachandran, M., & Sanjeeviraja, C. Intercalation studies on electron beam evaporated MoO_3 films for electrochemical devices. Solar Energy Materials and Solar Cells, 90(15), 2438–2448. (2006). DOI: 10.1016/j.solmat.2006.03.016

[12] Shaaban, K. S., Abo-Naf, S. M., & Hassouna, M. E. M. Physical and Structural Properties of Lithium Borate Glasses Containing MoO_3. Silicon **11,** 2421–2428, (2019). DOI:10.1007/s12633-016-9519-4

[13] Shaaban, K. S., Abo-naf S. M., Abd Elnaeim, A. M., & Hassouna, M. E. M. Studying effect of MoO_3 on elastic and crystallization behavior of lithium diborate glasses. Applied Physics A, 123(6) 457, (2017). DOI:10.1007/s00339-017-1052-9

[14] Rao, L. S., Reddy, M. S., Rao, D. K., & Veeraiah, N. Influence of redox behavior of copper ions on dielectric and spectroscopic properties of $Li_2O–MoO_3–B_2O_3$: CuO glass system. Solid-State Sciences, 11(2), 578–587. (2009). DOI: 10.1016/j.solidstatesciences.2008.06.022

[15] Shaaban, K. S., & Saddeek, Y. B. Effect of MoO_3 Content on Structural, Thermal, Mechanical and Optical Properties of (B_2O_3-SiO_2-Bi_2O_3-Na_2O-Fe_2O_3) Glass System. Silicon, 9(5), 785–793, (2017). DOI 10.1007/s12633-017-9558-5

[16] Shaaban, K.S., Zahran, H.Y., Yahia, I.S. *et al.* Mechanical and radiation-shielding properties of B_2O_3–P_2O_5–Li_2O–MoO_3 glasses. Appl. Phys. *A* **126,** 804 (2020). https://doi.org/10.1007/s00339-020-03982-9

[17] Elbers, S., Strojek, W., Koudelka, L., & Eckert, H. Site connectivities in silver borophosphate glasses: new results from 11B{31P} and 31P{11B} rotational echo double resonance NMR spectroscopy. Solid-State Nuclear Magnetic Resonance, 27(1-2), 65–76. (2005). DOI: 10.1016/j.ssnmr.2004.08.007

[18] Tricot, G., Alpysbay, L., & Doumert, B. Solid State NMR: A Powerful Tool for the Characterization of Borophosphate Glasses. Molecules, 25(2), 428. (2020). DOI:10.3390/molecules25020428

[19] Koudelka, L., & Mošner, P. Study of the structure and properties of Pb–Zn borophosphate glasses. Journal of Non-Crystalline Solids, 293-295, 635–641. (2001). DOI:10.1016/s0022-3093(01)00765-7

[20] Aldo Magistris, Gaetano Chiodelli, Silver borophosphate glasses : Ion transport, thermal stability and electrochemical behaviour, Solid State Ionics 9–10, (1), 611-615,1983, doi.org/10.1016/0167-2738(83)90303-X

[21] Manzani, D., de Araújo, C. B., Boudebs, G., Messaddeq, Y., & Ribeiro, S. J. L. The Role of Bi_2O_3 on the Thermal, Structural, and Optical Properties of Tungsten-Phosphate Glasses. The Journal of Physical Chemistry B, 117(1), 408–414. (2012). DOI:10.1021/jp3097296

[22] Taher, A. E., Ali, A. M., Saddeek, Y. B., Elsaman, R., Algarni, H., Shaaban, K., & Amer, T. Z. Gamma ray shielding and structural properties of iron alkali alumino-phosphate glasses modified by PbO. Radiation Physics and Chemistry,165, 108403. (2019). DOI: 10.1016/j.radphyschem.2019.108403

[23] Tsuchiya, T., & Moriya, T. Anomalous behavior of physical and electrical properties in borophosphate glasses containing R_2O and V_2O_5. Journal of Non-Crystalline Solids, 38-39, 323–328. (1980). DOI:10.1016/0022-3093(80)90439-1

[24] Møller, A.P., Mousseau, T.A., The effects of natural variation in background radioactivity on humans, animals and other organisms. Biol. Rev. 88, 226–254. (2013), https://doi.org/10.1111/j.1469-185X.2012.00249.x

[25] Mettler Jr., F.A., Huda, W., Yoshizumi, T.T., Mahesh, M., Effective doses in radiology and diagnostic nuclear medicine: a catalog. Radiology 248, 254–263. (2008), doi: 10.1148/radiol.2481071451

[26] Tekin H.O., Kavaz E., Papachristodoulou A., Kamislioglu M., O. Agar, E.E. Altunsoy Guclu, Kilicoglu O., Sayyed M.I., Characterization of SiO_2–PbO–CdO–Ga_2O_3 glasses for comprehensive nuclear shielding performance: alpha, proton, gamma, neutron radiation, Ceram. Int.45.15, 19206-19222, (2019), https://doi.org/10.1016/j.ceramint.2019.06.168

[27] Nowak M., Sans-Merce M., Lemesre C., Elmiger R., Damet J., Eye lens monitoring programme for medical staff involved in fluoroscopy guided interventional procedures in Switzerland, Phys. Med.57, 33-40. (2019), doi: 10.1016/j.ejmp.2018.12.001

[28] König A., Etzel R., Thomas R., Mahnken A., Personal Radiation Protection and Corresponding Dosimetry in Interventional Radiology: an Overview and Future

Developments, RöFo - Fortschritte Auf Dem Gebiet Der Röntgenstrahlen Und Der Bildgebenden Verfahren, 191(06), 512-521. (2019), doi: 10.1055/a-0800-0113

[29] Kosaka H., Monzen H., Matsumoto K., Tamura M., Nishimura Y., Reduction of operator hand exposure in interventional radiology with a novel finger sack using tungsten-containing rubber, Health Phys. 116(5), 625-630. (2019), doi: 10.1097/HP.0000000000000992

[30] Etzel R., König A.M., Keil B., Fiebich M., Mahnken A.H., Effectiveness of a new radiation protection system in the interventional radiology setting, Eur. J. Radiol. 106. 56-61. (2018), (2018), doi: 10.1016/j.ejrad.2018.07.006

[31] Chida K., Kaga Y., Haga Y., Kataoka N., Kumasaka E., Meguro T., Zuguchi, M., Occupational dose in interventional radiology procedures, Am. J. Roentgenol. 200(1), 138 - 141. (2013), doi: 10.2214/AJR.11.8455

[32] Kavaz E., Tekin H.O., Agar O., Altunsoy E.E., Kilicoglu O., Kamislioglu M., Abuzaid M.M., Sayyed M.I., The Mass stopping power/projected range and nuclear shielding behaviors of barium bismuth borate glasses and influence of cerium oxide, Ceram. Int. 45. (12,15), 15348-15357. (2019), DOI: 10.1016/j.ceramint.2019.05.028

[33] Kalnins C.A.G., Ebendorff-Heidepriem H., Spooner N.A., Monro T.M., Enhanced radiation dosimetry of fluoride phosphate glass optical fbres by terbium (III) doping, Opt. Mater. Express 6 (12), 3692-3703 (2016), https://doi.org/10.1364/OME.6.003692

[34] Şakar, E., Özpolat, Öü.F1., Alım, Bü., Sayyed, M.I., Kurudirek, M., PhyX / PSD: Development of a user-friendly online software for calculation of parameters relevant to radiation shielding and dosimetry, Radiation Physics and Chemistry 166, 108496. (2020), https://doi.org/10.1016/j.radphyschem.2019.108496

[35] Shaaban, K.S., Wahab, E.A.A., Shaaban, E.R., et al. Electronic Polarizability, Optical Basicity, Thermal, Mechanical and Optical Investigations of ($65B_2O_3–30Li_2O–5Al_2O_3$)

Glasses Doped with Titanate. Journal of Elec Materi **49,** 2040–2049 (2020). https://doi.org/10.1007/s11664-019-07889-x

[36] Abdelghany, A. M., ElBatal, F. H., Azooz, M. A., Ouis, M. A., & ElBatal, H. A. Optical and infrared absorption spectra of 3d transition metal ions-doped sodium borophosphate glasses and effect of gamma irradiation. Spectrochimica Acta Part A: Molecular and Biomolecular Spectroscopy, 98, 148–155. (2012). DOI: 10.1016/j.saa.2012.08.049

[37] Abd-Allah, W.M., Saudi, H.A., Shaaban, K.S. *et al.* Investigation of structural and radiation shielding properties of $40B_2O_3$–$30PbO$–$(30$-$x)$ BaO-x ZnO glass system. Appl. Phys. A **125,** 275 (2019). https://doi.org/10.1007/s00339-019-2574-0

[38] Saudi, H.A., Abd-Allah, W.M. & Shaaban, K.S. Investigation of gamma and neutron shielding parameters for borosilicate glasses doped europium oxide for the immobilization of radioactive waste. J Mater Sci: Mater Electron **31,** 6963–6976 (2020). https://doi.org/10.1007/s10854-020-03261-6

[39] Abdel Wahab, E.A., Shaaban, K.S., Elsaman, R. *et al.* Radiation shielding, and physical properties of lead borate glass doped ZrO_2 nanoparticles. Appl. Phys. A (12) **125,** 869 (2019). https://doi.org/10.1007/s00339-019-3166-8

[40] Shaaban, K., Abdel Wahab, E.A., El-Maaref, A.A. et al. Judd–Ofelt analysis and physical properties of erbium modified cadmium lithium gadolinium silicate glasses. J Mater Sci: Mater Electron **31,** 4986–4996 (2020). https://doi.org/10.1007/s10854-020-03065-8

[41] Shaaban, K.S., Koubisy, M.S.I., Zahran, H.Y. et al. Spectroscopic Properties, Electronic Polarizability, and Optical Basicity of Titanium–Cadmium Tellurite Glasses Doped with Different Amounts of Lanthanum. J Inorg Organomet Polym (2020). https://doi.org/10.1007/s10904-020-01640-4

[42] Somaily, H.H., Shaaban, K.S., Makhlouf, S.A. *et al.* Comparative Studies on Polarizability, Optical Basicity and Optical Properties of Lead Borosilicate Modified with Titania. J Inorg Organomet Polym (2020). https://doi.org/10.1007/s10904-020-01650-2

[43] Shaaban, K. S., El Sayed Yousef, Optical properties of Bi_2O_3 doped borotellurite glasses and glass-ceramics. Optik - International Journal for Light and Electron Optics 203, 163976. (2020), https://doi.org/10.1016/j.ijleo.2019.163976

[44] Wahab, E. A. A., & Shaaban, K. S. Effects of SnO_2 on spectroscopic properties of borosilicate glasses before and after plasma treatment and its mechanical properties. Materials Research Express, 5(2), 025207, (2018). https://doi.org/10.1088/2053-1591/aaaee8

[45] Dimitrov, V., & Sakka, S. (1996). Electronic oxide polarizability and optical basicity of simple oxides. I. Journal of Applied Physics, **79**(3) 1736. doi.org/10.1063/1.360962

 [46] Dimitrov, V., & Komatsu, T. (2002). Classification of Simple Oxides: A Polarizability Approach.   Journal   of   Solid-State   Chemistry,   **163**(1)   100. https://doi.org/10.1006/jssc.2001.9378

[47] Zhao, X., Wang, X., Lin, H., & Wang, Z. (2007). Electronic polarizability and optical basicity of lanthanide oxides. Physica B: Condensed Matter, 392(1-2), 132–136. 10.1016/j.physb.2006.11.015

[48] Duffy, J. A. (1989). A common optical basicity scale for oxide and fluoride glasses. Journal of Non-Crystalline Solids, 109(1), 35–39, https://doi.org/10.1016/0022-3093(89)90438-9

[49] Duffy, J. A., & Ingram, M. D. (1992). Comments on the application of optical basicity to glass. Journal of Non-Crystalline Solids, 144, 76–80. doi:10.1016/s0022-3093(05)80385-0

[50] Wemple S.H., Didomenico M., Behavior of the Electronic Dielectric Constant in Covalent and Ionic Materials, Phys. Rev. B 3, 1338 (1971).

[51] Abdel-Aziz, M. M., Yahia, I. S., Wahab, L. A., Fadel, M., & Afifi, M. A. Determination and analysis of dispersive optical constant of TiO_2 and Ti_2O_3 thin films. Appl. Sur. Sci., 252(23), 8163–8170, (2006).

[52] Abdel-Aziz, M. M., Metwally E.G. El-, Fadel M., Labib H.H., Afifi, M. A., Optical properties of amorphous Ge-Se-Tl system films, Thin Solid Films 386, 99 – 104, (2001).

[53] Chiad S. S., Habubi, N. F., Abass W. H., Abdul Allah M. H., Effect of thickness on the optical and dispersion parameters of $Cd_{0.4}Se_{0.6}$ thin films, J. of opt. elec. and adv. mat., **18**, (9-10), 822 (2016).

[54] El-Sharkawy, R. M., Shaaban, K. S., Elsaman, R., Allam, E. A., El-Taher, A., & Mahmoud, M. E. Investigation of mechanical and radiation shielding characteristics of novel glass systems with the composition $xNiO$-$20ZnO$-$60B_2O_3$-$(20-x)$ CdO based on nano metal oxides. Journal of Non-Crystalline Solids, 528,119754, (2020), DOI: 10.1016/j.jnoncrysol.2020.

[55] El-Rehim, A.A., Zahran, H., Yahia, I. *et al.* (2020) Radiation, Crystallization, and Physical Properties of Cadmium Borate Glasses. Silicon. https://doi.org/10.1007/s12633-020-00798-3

[56] Singh, T., Kaur, P., & Singh, P. S. Variation of Mass Attenuation Coefficient, Effective Atomic Number, and Electron Density with Incident Photon Energy of Some Organic Acids. Nuclear Science and Engineering, 156(2), 229–243. (2007). DOI:10.13182/nse07-a2699

[57] Singh, K., Singh, H., Sharma, G., Gerward, L., Khanna, A., Kumar, R., Sahota, H. S. Gamma-ray shielding properties of CaO–SrO–B_2O_3 glasses. Radiation Physics and Chemistry, 72(2-3), 225–228. (2005). DOI: 10.1016/j.radphyschem.2003.11.010

[58] Mostafa, A. G., Hassaan, M. Y., Ramadan, A. B., Hussein, A. Z., & Abdel-Haseib, A. Y. Characterization of iron sodium phosphate glasses doped Ba^{2+} cations for using as radioactive waste encapsulation. Nature and Sci, 11, 148-155. (2013). http://www.sciencepub.net/nature.

[59] Waly, E.-S. A., Fusco, M. A., & Bourham, M. A. Gamma-ray mass attenuation coefficient and half value layer factor of some oxide glass shielding materials. Annals of Nuclear Energy, 96, 26–30. (2016). DOI: 10.1016/j.anucene.2016.05.028

[60] Tekin, H. O., Kavaz, E., Papachristodoulou, A., Kamislioglu, M., Agar, O., Altunsoy Guclu, E. E., Sayyed, M. I. Characterization of SiO2–PbO–CdO–Ga2O3 glasses for comprehensive nuclear shielding performance: Alpha, proton, gamma, neutron radiation. Ceramics International 45, 19206–19222, (2019) DOI: 10.1016/j.ceramint.2019.06.168

[61] Rammah, Y. S., Abouhaswa, A. S., Sayyed, M. I., Tekin, H. O., & El-Mallawany, R. Structural, UV and shielding properties of ZBPC glasses. Journal of Non-Crystalline Solids. DOI: 10.1016/j.jnoncrysol.2018.12.013

[62] Kavaz, E., Tekin, H. O., Agar, O., Altunsoy, E. E., Kilicoglu, O., Kamislioglu, M., Sayyed, M. I. The Mass stopping power / projected range and nuclear shielding behaviors of barium bismuth borate glasses and influence of cerium oxide. Ceramics International 45, 15348–15357, (2019) doi: 10.1016/j.ceramint.2019.05.028

[63] Issa, S. A. M., Saddeek, Y. B., Tekin, H. O., Sayyed, M. I., & Shaaban, K. saber. Investigations of radiation shielding using Monte Carlo method and elastic properties of PbO-SiO_2-B_2O_3-Na_2O glasses. Current Applied Physics, 18(6), 717–727. (2018). DOI: 10.1016/j.cap.2018.02.018

[64] Issa, S. A. M., Tekin, H. O., Elsaman, R., Kilicoglu, O., Saddeek, Y. B., & Sayyed, M. I. Radiation shielding and mechanical properties of Al_2O_3–Na_2O–B_2O_3−Bi_2O_3 glasses using MCNPX Monte Carlo code. Materials Chemistry and Physics. 223, 1 ,209-219 (2019), DOI: 10.1016/j.matchemphys.2018.10.064

[65] Tekin, H. O., Kilicoglu, O., Kavaz, E., Altunsoy, E. E., Almatari, M., Agar, O., & Sayyed, M. I. The investigation of gamma-ray and neutron shielding parameters of Na_2O-CaO-P_2O_5-SiO_2 bioactive glasses using MCNPX code. Results in Physics 12 1797–1804. (2019). DOI: 10.1016/j.rinp.2019.02.017

[66] Kaur, P., Singh, D., & Singh, T. Heavy metal oxide glasses as gamma rays shielding material. Nuclear Engineering and Design, 307, 364–376. (2016). doi: 10.1016/j.nucengdes.2016.07.029

[67] Sayyed, M.I., Laariedh, F., Kumr, A. *et al.* Experimental studies on the gamma photons-shielding competence of TeO_2–PbO–BaO–Na_2O–B_2O_3 glasses. Appl. Phys. A **126,** 4 (2020). https://doi.org/10.1007/s00339-019-3182-8

[68] Agar O, Sayyed MI, Tekin HO, Kaky KM, Baki SO, Kityk I. An investigation on shielding properties of BaO, MoO_3 and P_2O_5 based glasses using MCNPX code. Results Phys 2019; 12:629–34. https://doi.org/10.1016/j.rinp.2018.12.003

 [69] Rammah, Y.S., El-Agawany, F.I., Mahmoud, K.A. *et al.* FTIR, UV–Vis–NIR spectroscopy, and gamma rays shielding competence of novel ZnO-doped vanadium borophosphate glasses. J Mater Sci: Mater Electron (2020). https://doi.org/10.1007/s10854-020-03440-5

[70] Matori, K. A., Sayyed, M. I., Sidek, H. A. A., Zaid, M. H. M., & Singh, V. P. Comprehensive study on physical, elastic and shielding properties of lead zinc phosphate glasses. Journal of Non-Crystalline Solids, 457, 97–103. (2017). DOI: 10.1016/j.jnoncrysol.2016.11.029

[71] Rammah, Y. S., Mahmoud, K. A., Kavaz, E., Kumar, A., & El-Agawany, F. I. The role of PbO/Bi_2O_3 insertion on the shielding characteristics of novel borate glasses. Ceramics International. (2020). DOI: 10.1016/j.ceramint.2020.04.018

Figures
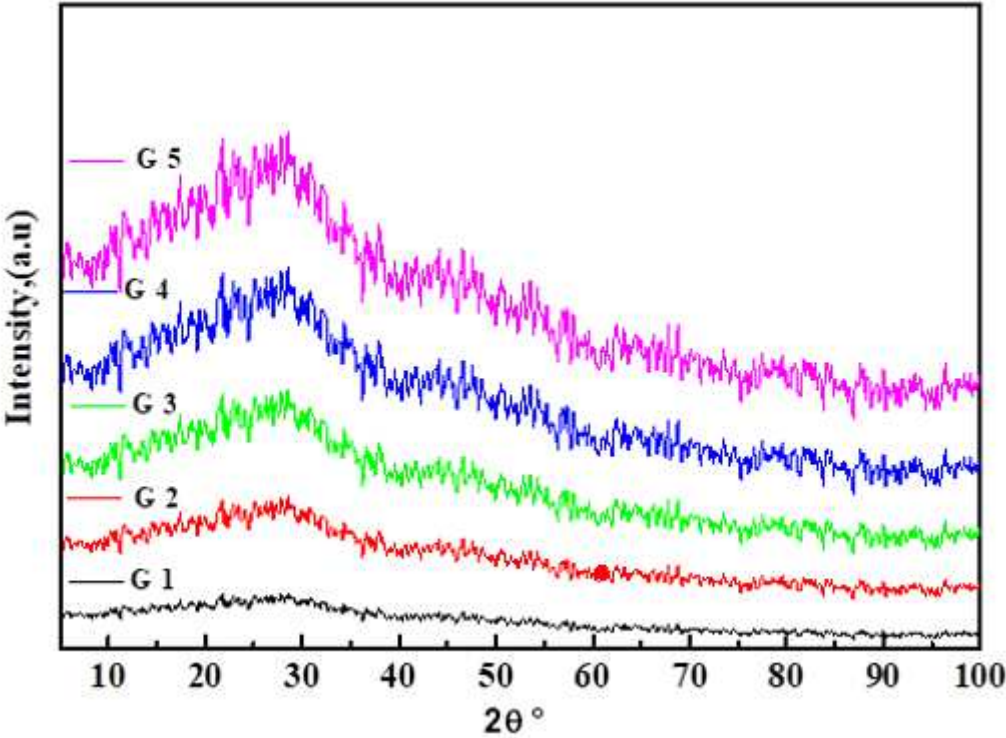
Figure 1

XRD of the studied glasses.
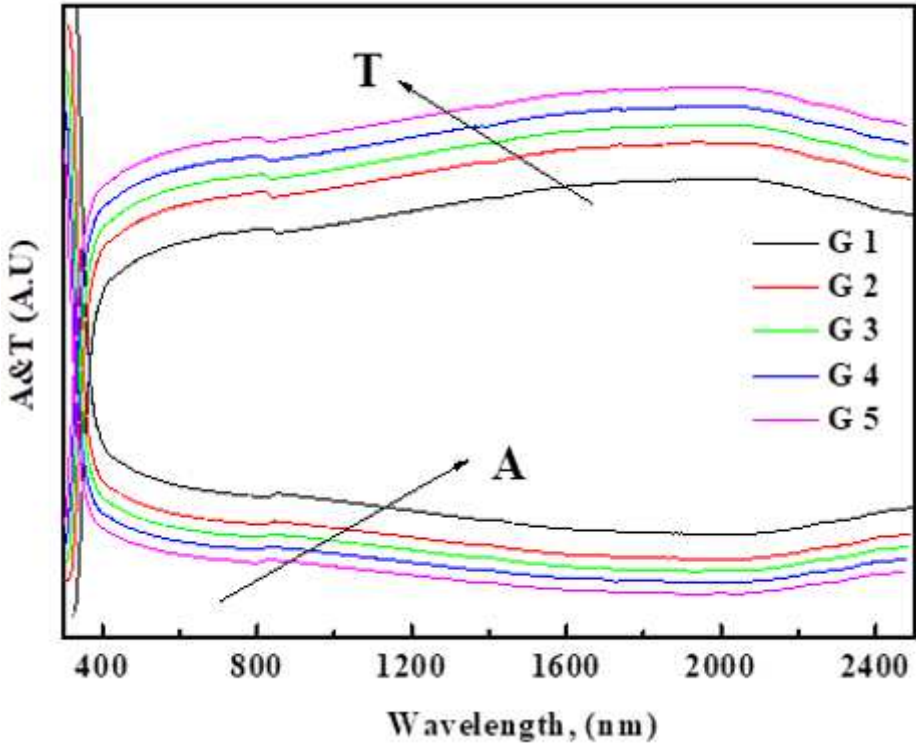
Figure 2

The absorbance (A) and Transmittance (T) of the prepared glasses.
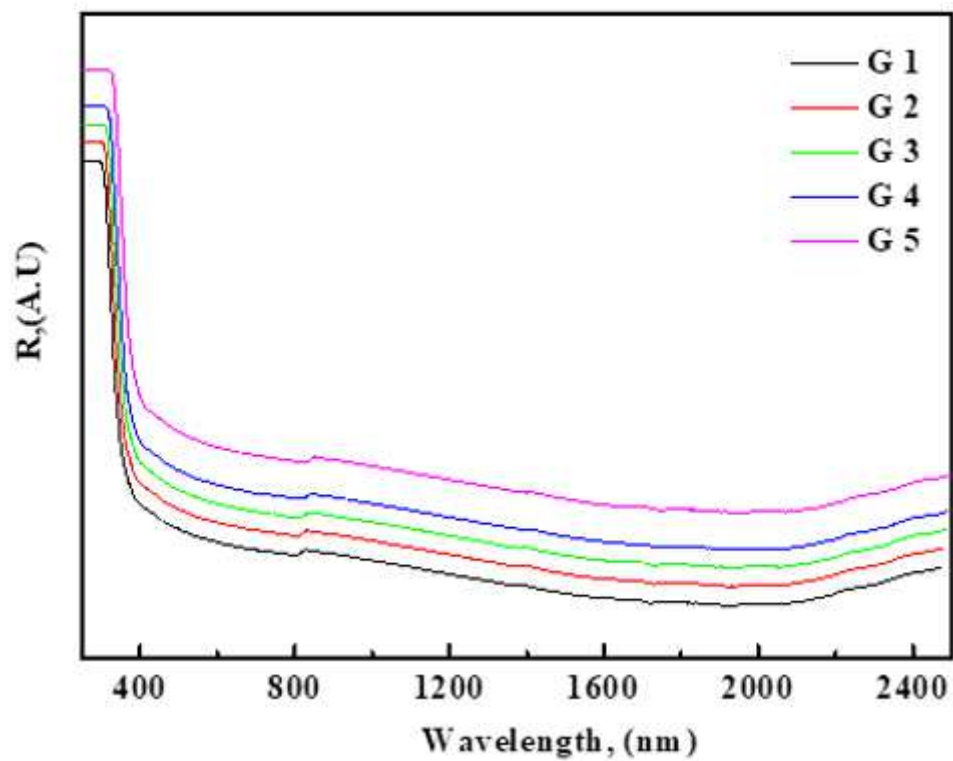
Figure 3

The reflectance (R) of the prepared glasses.
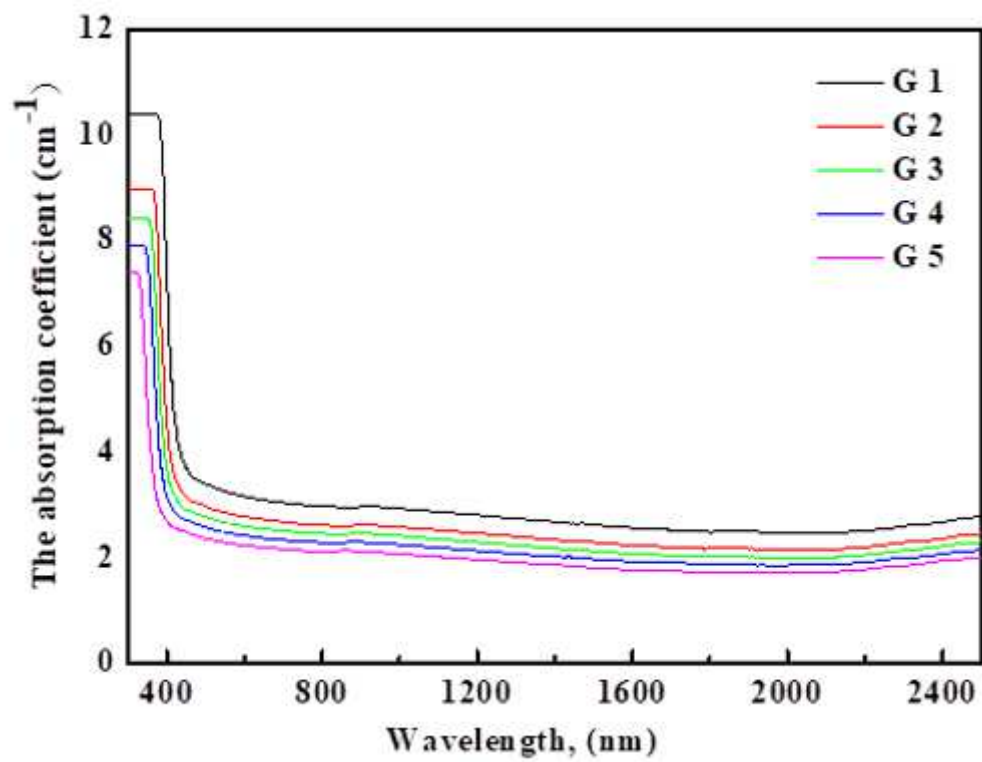
Figure 4

The absorption coefficient of the prepared glasses.
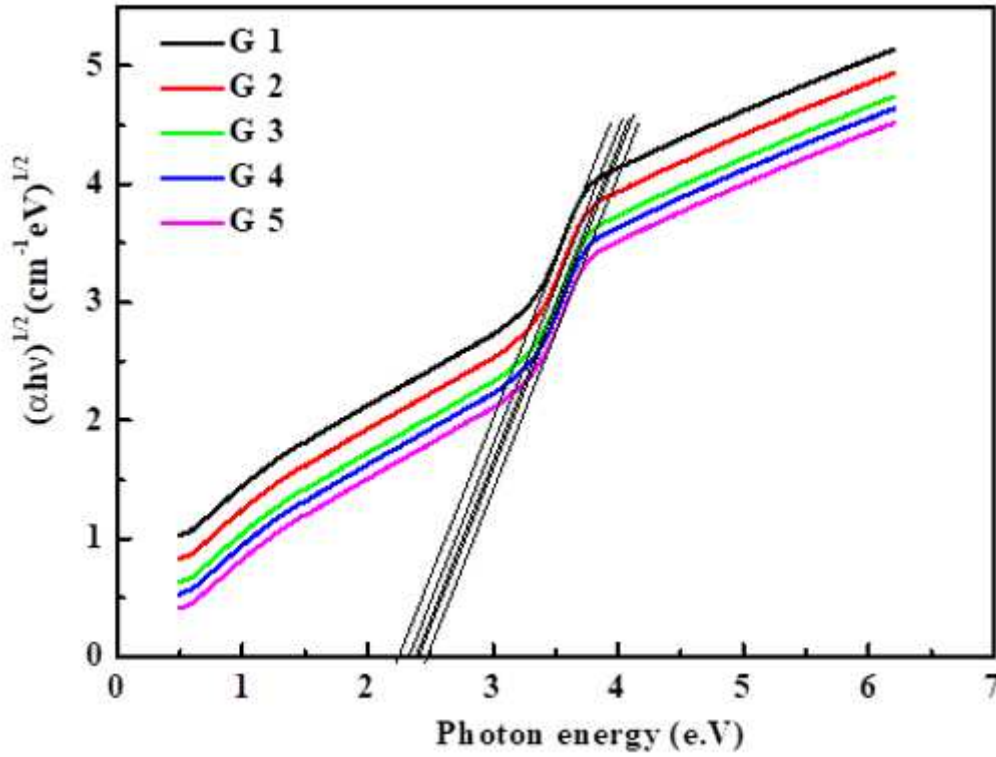
Figure 5

Plot of $(\alpha h\upsilon)^{1/2}$ against photon energy ($h\upsilon$) to calculate the indirect optical band gap from the intercept of the curves.
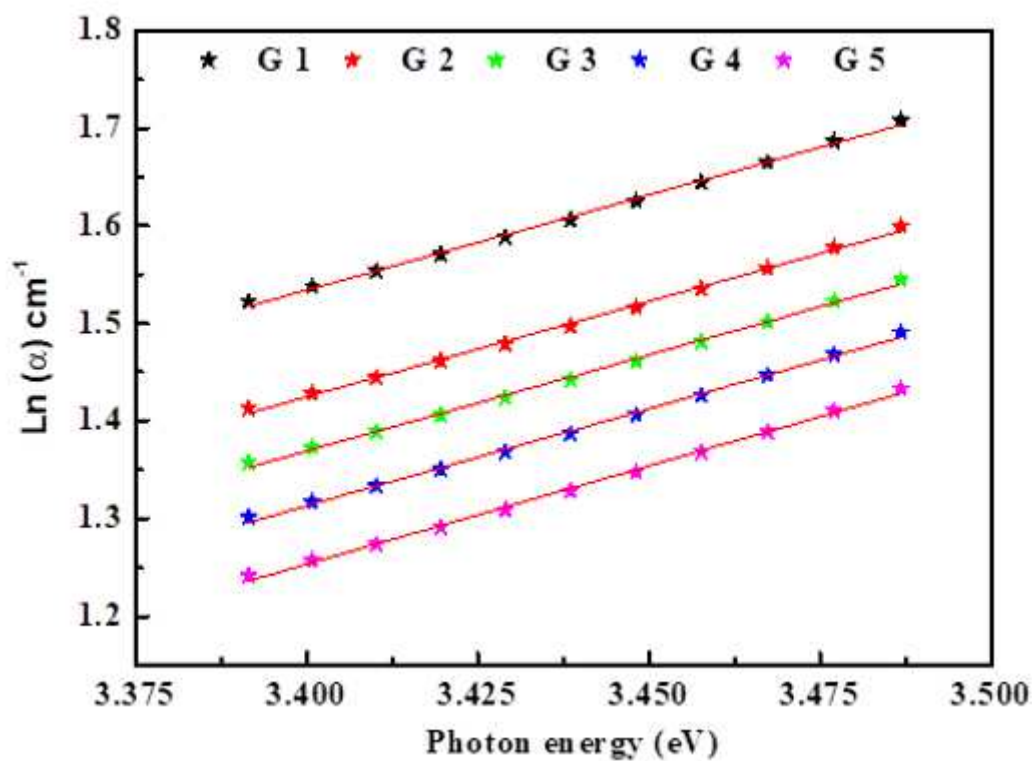
Figure 6

Dependence of ln(α) upon the photon energy (hυ) for the prepared glasses.
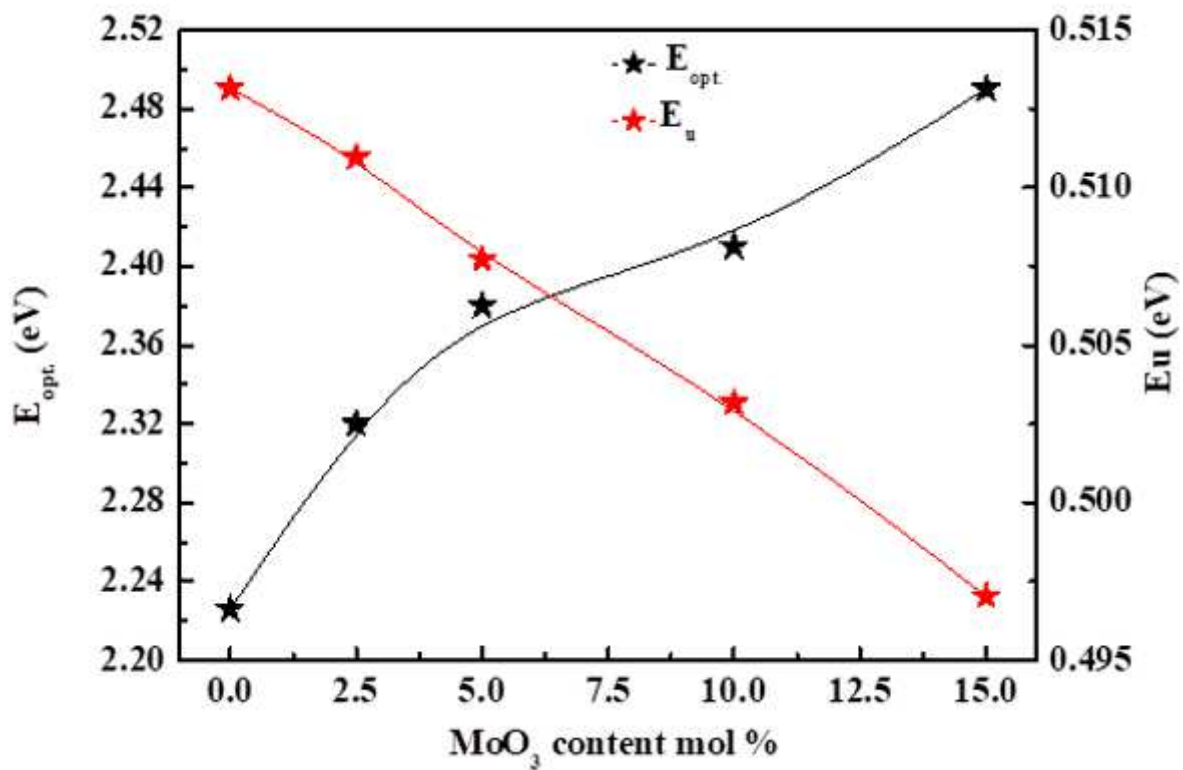
Figure 7

Optical band gap and Urbach energy versus concentration of MoO3.
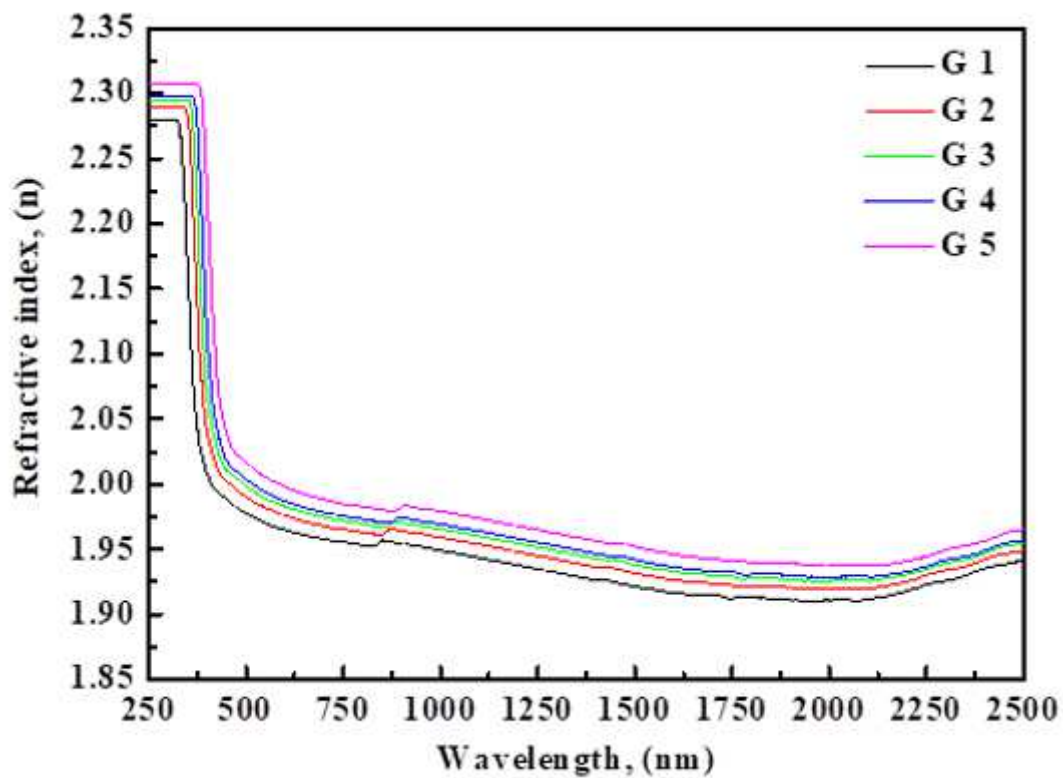
Figure 8

Refractive index of the prepared glasses.
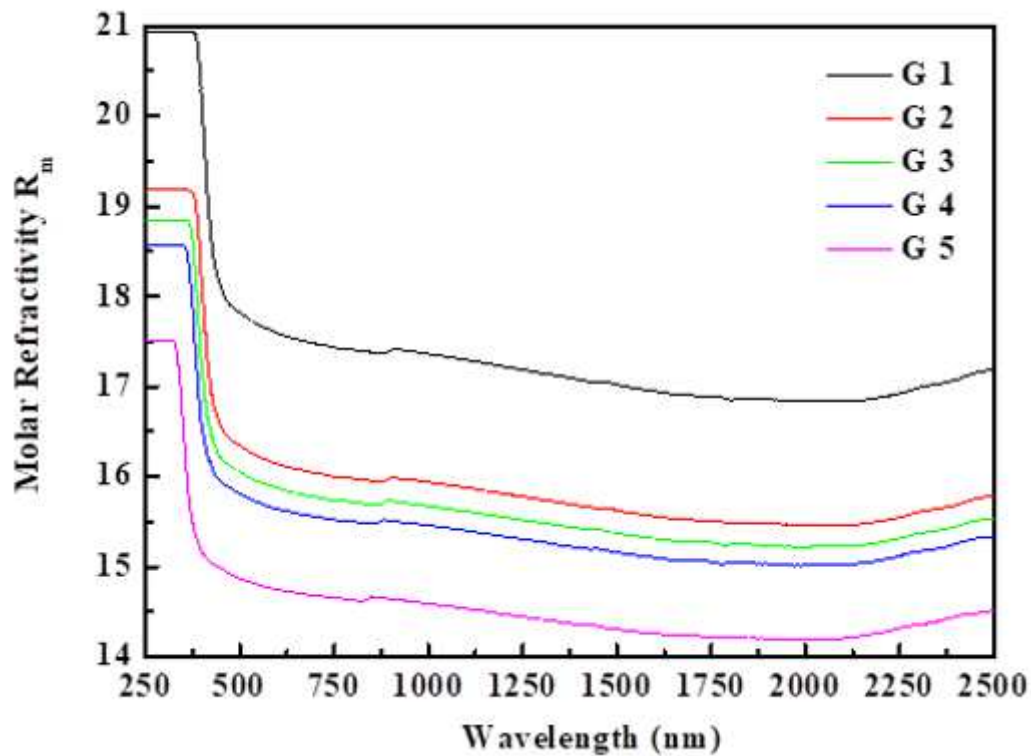
Figure 9

Molar refractivity of the prepared glasses.
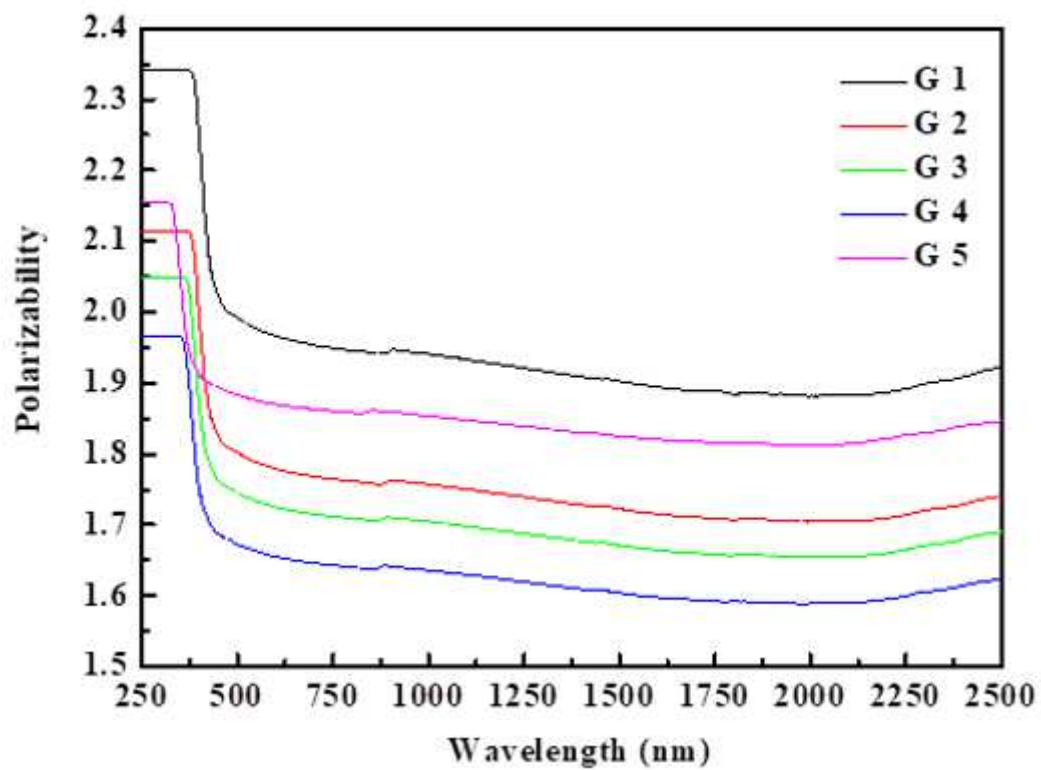
Figure 10

Electronic polarizability of the prepared glasses.
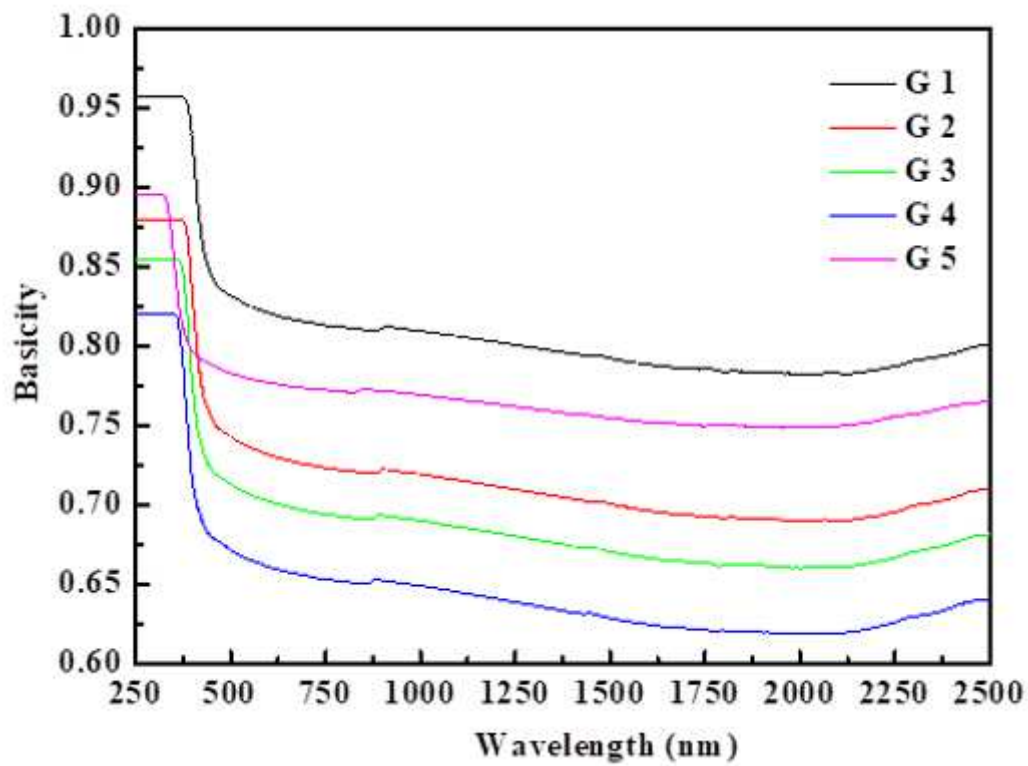
Figure 11

Optical basicity of the prepared glasses.
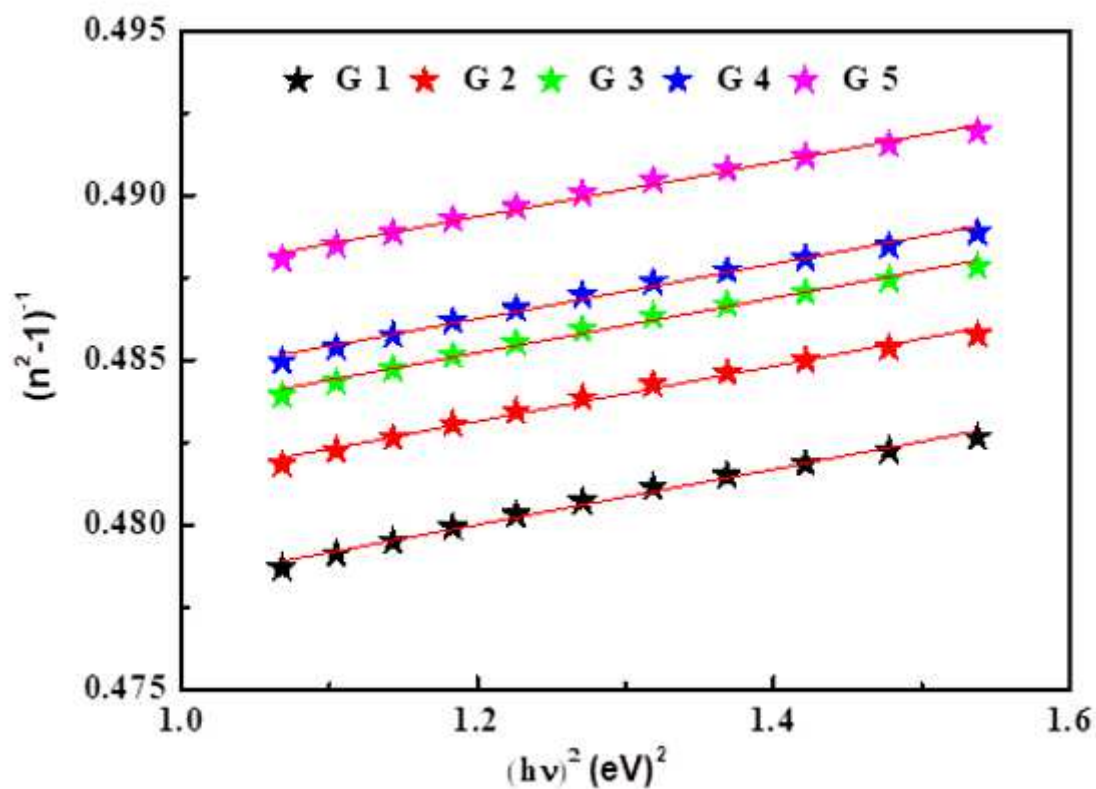
Figure 12

Variation of (n2-1)-1 with (hυ)2 for the prepared glasses.
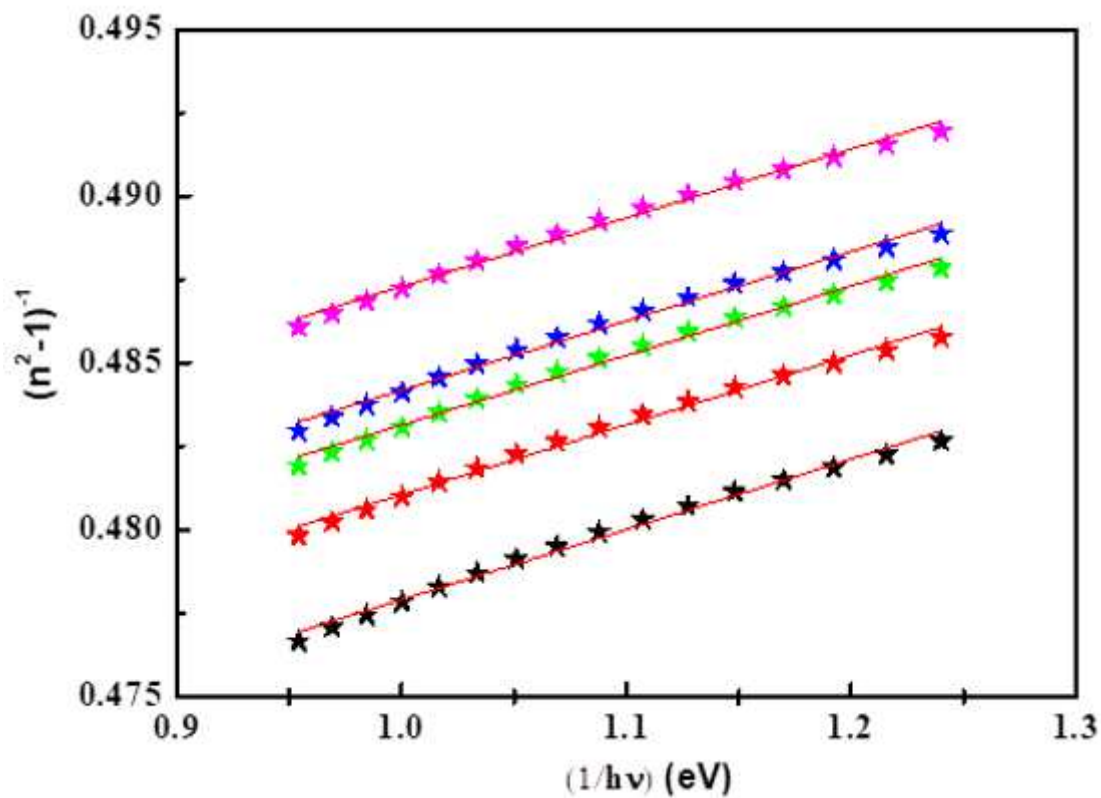
Figure 13

Variation of (n2-1)-1 with 1/(hυ) for the prepared glasses.
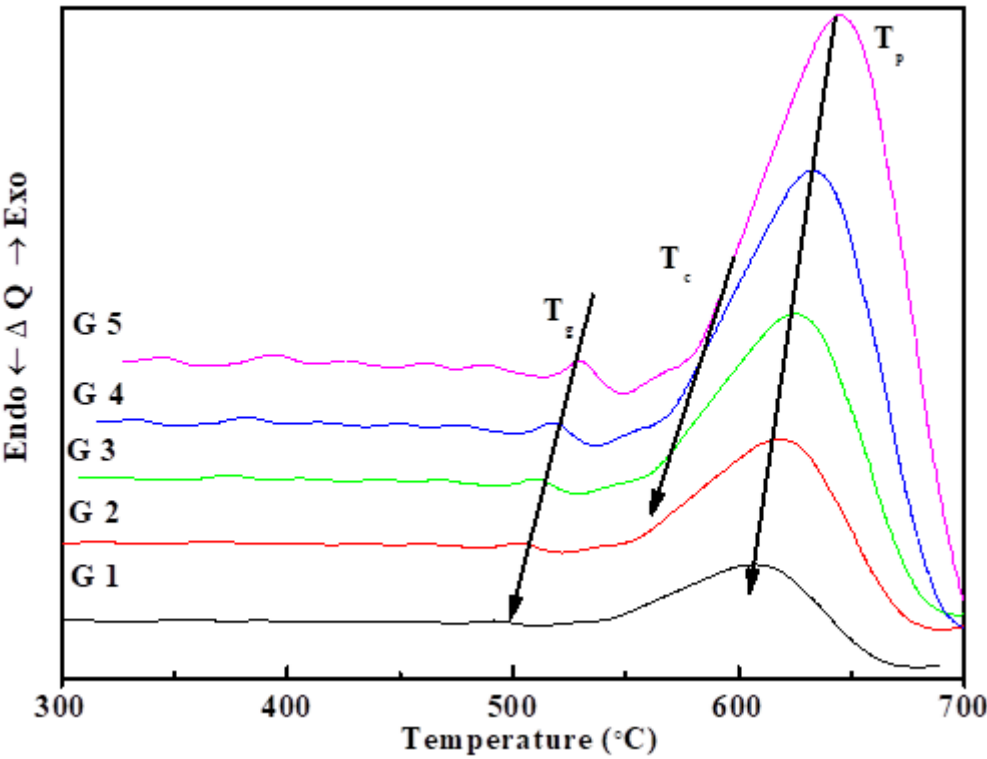
Figure 14

DTA of the prepared glasses.
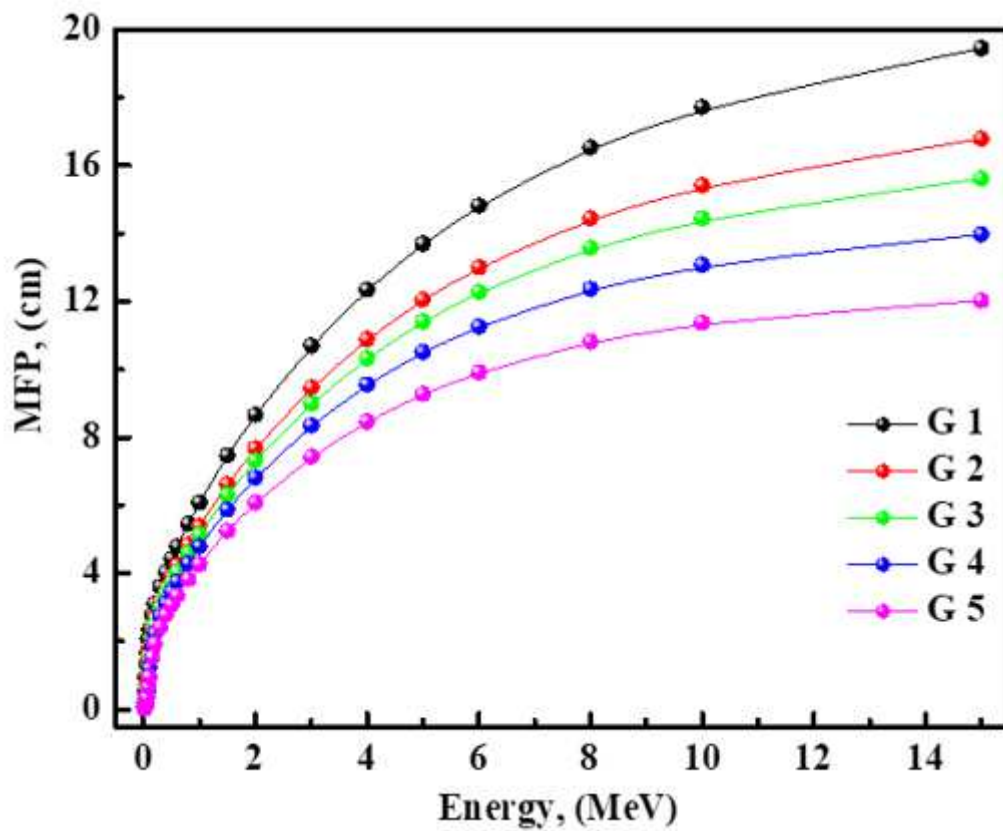
Figure 15

The MFP for the prepared glasses as a function of photon energy.
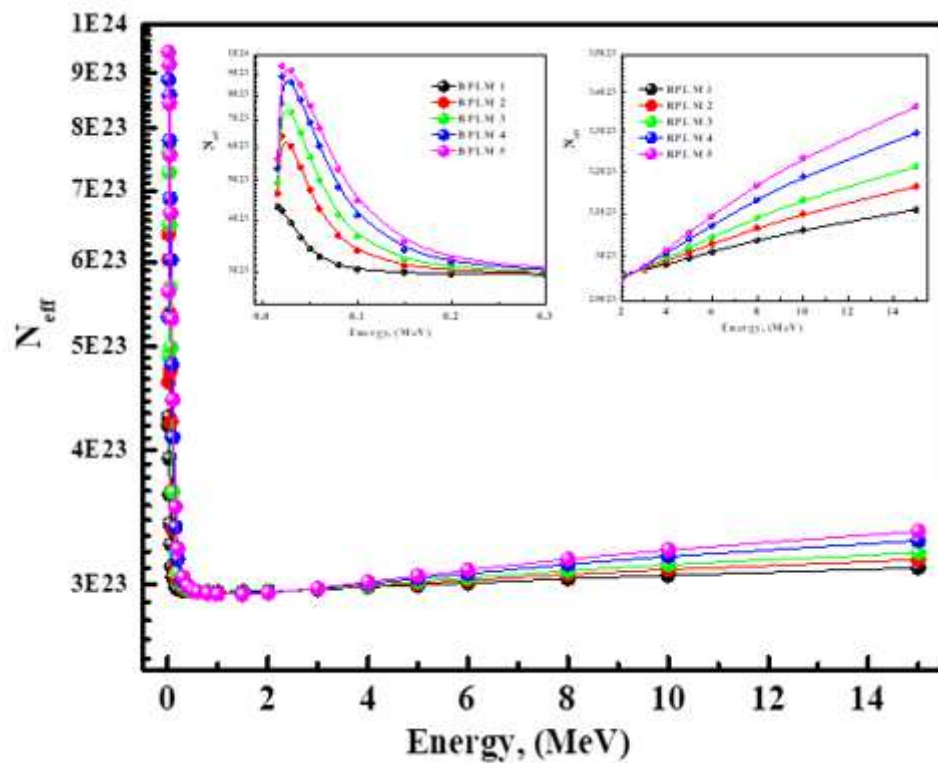
Figure 16

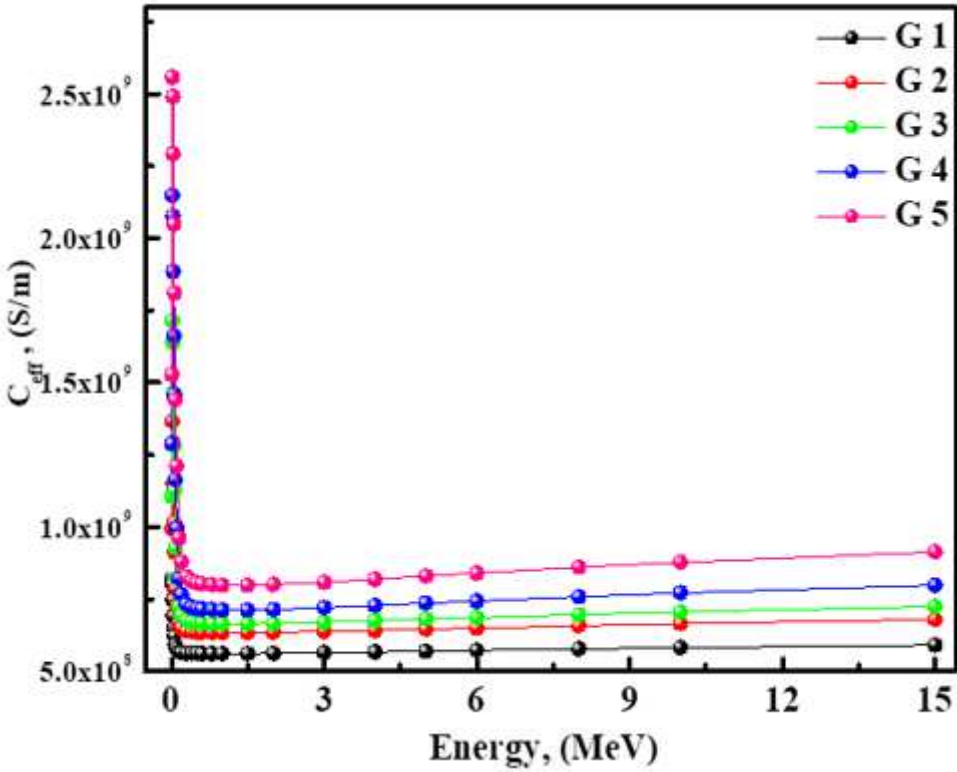The (Neff) for the prepared glasses as a function of photon energy.
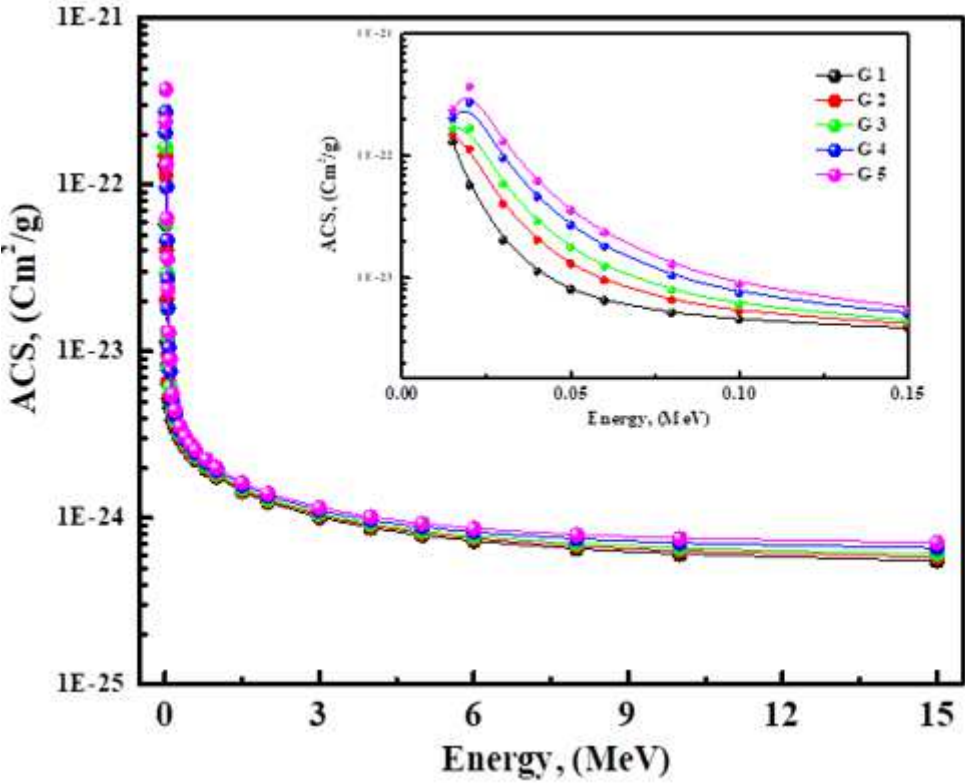
Figure 17

The ASC for the prepared glasses as a function of photon energy

Figure 18

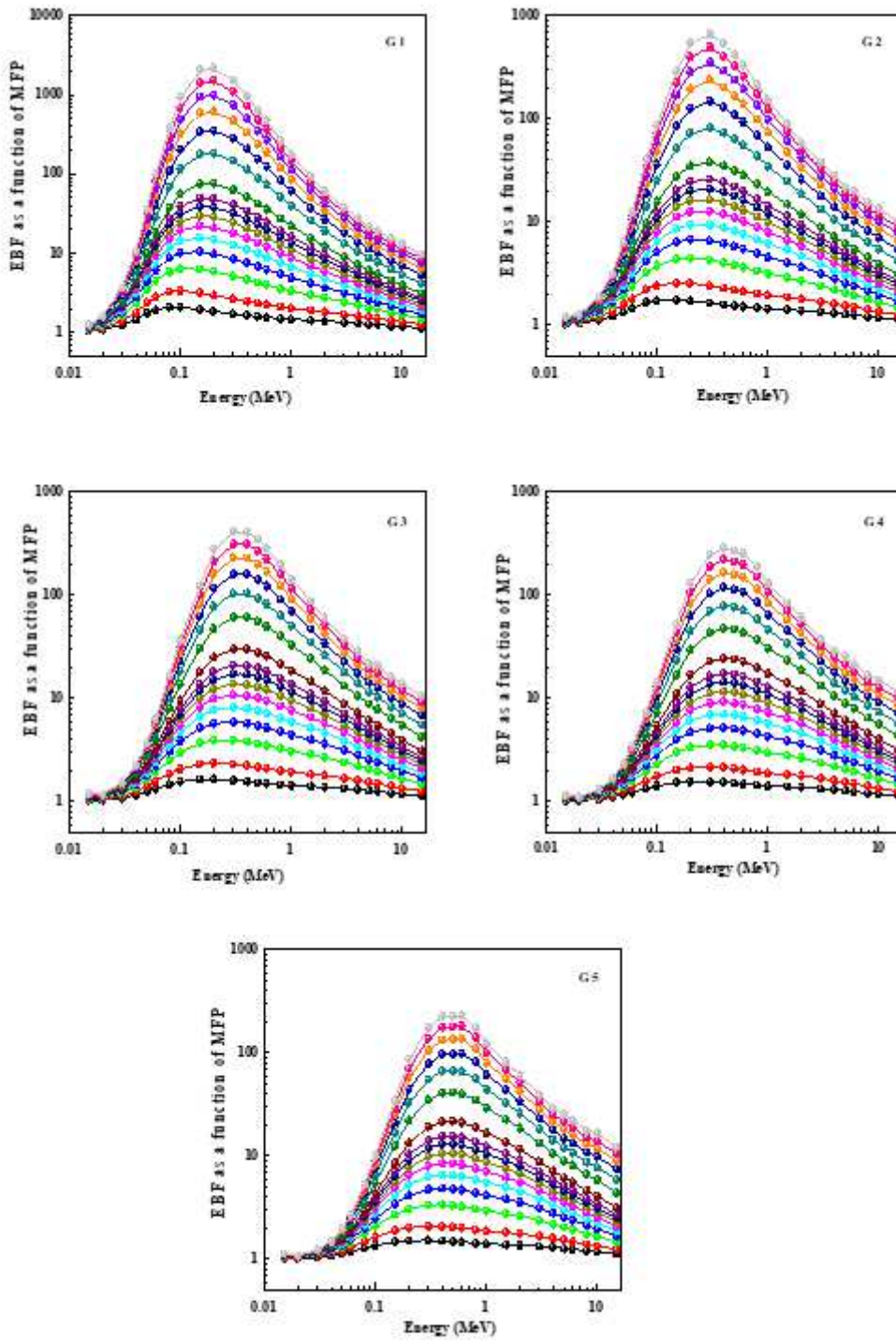The Ceff for the prepared glasses as a function of photon energy.

Figure 19

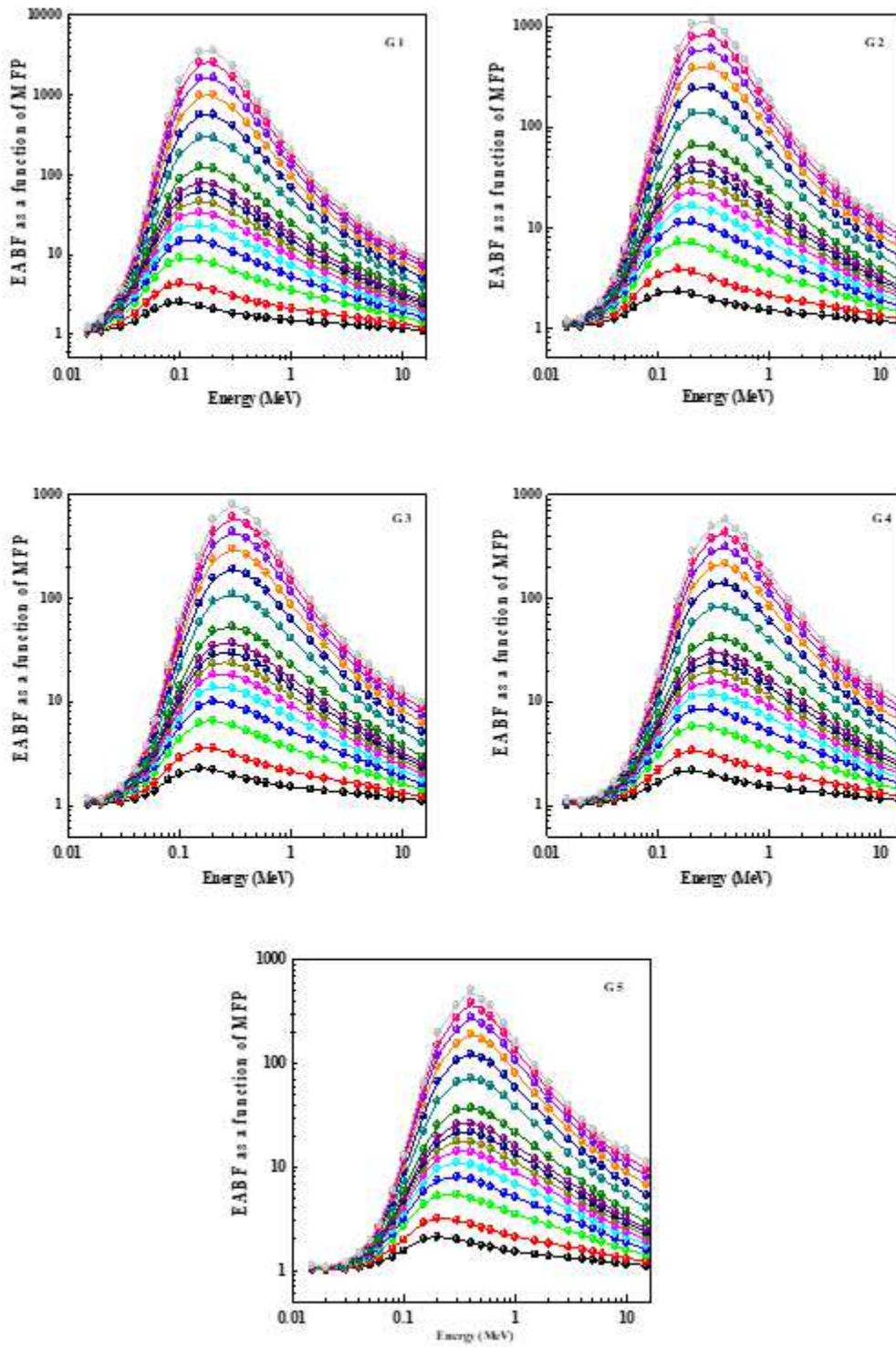Variation of EBF versus the gamma ray energy for the prepared glasses as a function of photon energy.

Figure 20

Variation of EABF versus the gamma ray energy for the prepared glasses as a function of photon energy.
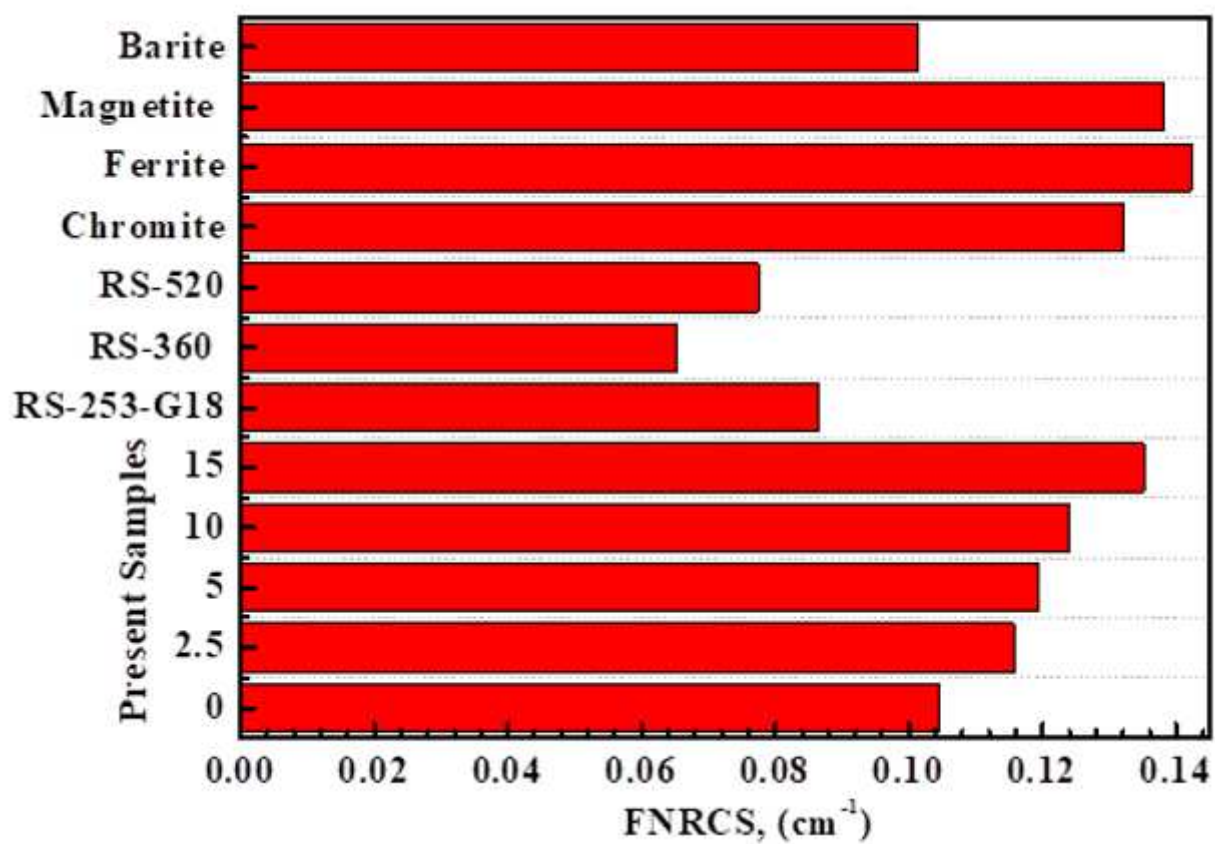
Figure 21

FNRCS for the prepared glasses comparison with standard materials.